*nanomaterials*

MDPI

*Article*

# Temperature Control of Yellow Photoluminescence from $SiO_2$-Coated ZnO Nanocrystals

**Narender Kumar [1], Vijo Poulose [1], Youssef Taiser Laz [2], Falguni Chandra [1], Salma Abubakar [3], Abdalla S. Abdelhamid [1], Ahmed Alzamly [1] and Na'il Saleh [1,*]**

[1] Department of Chemistry, College of Science, United Arab Emirates University, Al Ain P.O. Box 15551, United Arab Emirates
[2] Academic Support Department, Abu Dhabi Polytechnic, Al Ain P.O. Box 15551, United Arab Emirate
[3] Science Division, New York University Abu Dhabi (NYUAD), Saadiyat Island P.O. Box 129188, United Arab Emirates
* Correspondence: n.saleh@uaeu.ac.ae; Tel.: +971-3-713-6138

**Abstract:** In this study, we aimed to elucidate the effects of temperature on the photoluminescence from ZnO–$SiO_2$ nanocomposite and to describe the preparation of $SiO_2$-coated ZnO nanocrystals using a chemical precipitation method, as confirmed by Fourier transform infrared (FTIR) and powder X-ray diffraction analysis (XRD) techniques. Analyses using high-resolution transmission microscopy (TEM), energy-dispersive X-ray spectroscopy (EDX), dynamic light scattering (DLS), and electrophoretic light scattering (ELS) techniques showed that the new nanocomposite has an average size of 70 nm and 90% silica. Diffuse reflectance spectroscopy (DRS), photoluminescence (PL), and photoluminescence-excitation (PLE) measurements at different temperatures revealed two emission bands at 385 and 590 nm when the nanomaterials were excited at 325 nm. The UV and yellow emission bands were attributed to the radiative recombination and surface defects. The variable-temperature, time-resolved photoluminescence (VT-TRPL) measurements in the presence of $SiO_2$ revealed the increase in the exciton lifetime values and the interplay of the thermally induced nonradiative recombination transfer of the excited-state population of the yellow emission via deep centers (DC). The results pave the way for more applications in photocatalysis and biomedical technology.

**Keywords:** ZnO nanocrystals; temperature control; time-resolved photoluminescence; nonradiative relaxation

check for updates

**Citation:** Kumar, N.; Poulose, V.; Laz, Y.T.; Chandra, F.; Abubakar, S.; Abdelhamid, A.S.; Alzamly, A.; Saleh, N. Temperature Control of Yellow Photoluminescence from $SiO_2$-Coated ZnO Nanocrystals. *Nanomaterials* **2022**, *12*, 3368. https://doi.org/10.3390/nano12193368

Academic Editor: Junying Zhang

Received: 20 July 2022
Accepted: 25 September 2022
Published: 27 September 2022

**Publisher's Note:** MDPI stays neutral with regard to jurisdictional claims in published maps and institutional affiliations.

**Copyright:** © 2022 by the authors. Licensee MDPI, Basel, Switzerland. This article is an open access article distributed under the terms and conditions of the Creative Commons Attribution (CC BY) license (https://creativecommons.org/licenses/by/4.0/).

## 1. Introduction

In recent years, zinc oxide (ZnO) has gained significant attention because of its promising applications in photonics [1], spintronics [2], and optoelectronic devices such as LEDs (light emitting diodes) [3], phase-change memory devices [4], solar cells [5], sensors [6], antibacterial activity [7], plant growth [8], electrochemistry [9], and photocatalysts [10].

To prepare photoluminescent nanocomposites from ZnO, because ZnO alone tends to aggregate, researchers have used several techniques such as annealing, double-jet precipitation, spray-drying, and sol–gel methods to prepare ZnO–$SiO_2$ nanocomposites with pure UV emissions [11] at 360 and 400 nm [12], multicolored emission (from 460 to 550 nm) depending on the aging time [13], infrared emission via energy transfer to $Yb^{3+}$ [14], and multicolored emission from 365 to 517 nm depending on the calcination temperature [15]; all nanocomposites have been excited at 325 nm. Recently, due to the interesting photoluminescence (PL) properties of ZnO–$SiO_2$ films, many researchers have used nanomaterials as antidotes in human dermal fibroblast cells [16], as antibacterial agents [17], and as photocatalysts, which are one of the most popular applications [18].

The dependence of the photocatalytic activity of ZnO/$SiO_2$ nanomaterials on temperature [18,19] needs further elucidation. For instance, the temperature-dependent PL of ZnO/$SiO_2$ nanomaterials has never been investigated. Time-resolved photoluminescence (TRPL) spectroscopy is one the most important tools to investigate the bandgap, defect, and

impurity of any nanostructure or bulk material. The UV and visible PL of ZnO–$SiO_2$ films have already been attributed to radiative recombination and surface defects [11]. Here, we analyze TRPL measurements at different temperatures to understand the photophysical role of $SiO_2$ coating in generating nanocomposites with temperature-dependent PL aside from its role in increasing the exciton lifetime values [20]. The interplay of thermally induced nonradiative recombination transfer via deep centers (DC) of the excited-state population of the yellow emission band is confirmed.

## 2. Experimental Methods

### *2.1. Synthesis of Zinc Oxide Nanocrystals*

First, the ZnO nanoparticles were generated from a colloidal solution of ZnO in 250 mL ethanol before mixing them with 5.5 g of zinc acetate dehydrate (purity > 98% by Sigma-Aldrich, Saint Louis, MO, USA). Then, the final suspension was homogenized by heating under reflux for 1 h [21]. The distillation method was used to remove 150 mL of the solvent. After adding a new fresh volume of ethanol, 1.39 g of lithium hydroxide monohydrate (Aldrich) was added, and the new suspension was blended in an ultrasonic bath at 333 K. The dispersed mixture for 1 h was assumed to contain pure nanoparticles of ZnO, and then the mixture was filtered through a 0.1 mm membrane filter to remove undissolved LiOH. Then, the final white precipitate of the ZnO nanoparticles was heated in 100 mL of 10% deionized water in ethanol at 333 K, centrifuged, and then washed four times with an ethanol/water mixture (19:1) to remove residual ionic compounds [22].

### *2.2. Coating of ZnO Nanocrystals with $SiO_2$*

An amount of 0.5 g of ZnO was dispersed with silica (90 wt%), and then the resultant suspension was sonicated for 5 min, stirred overnight in LiOH by centrifugation, and washed four times with ethanol/water mixture (19:1) to remove residual ionic compounds, and then dried in a vacuum oven at 333 K.

### *2.3. Fourier Transform Infrared (FTIR) Spectroscopy*

Identification of the functional group was performed using a Thermo Scientific Nicolet instrument, and all samples were prepared using FTIR grade KBr which was sourced from Sigma-Aldrich. The samples were dispersed in water and physically scratched on a glass plate. The resulting water suspension was dried by evaporating water with the aid of a hot plate and an oven at 383 K, and then KBr was weighed quantitatively at a ratio of 1:100 (wt/wt).

### *2.4. High-Resolution Transmission Microscopy (HR-TEM)*

The internal morphology (final shape and length) of the $SiO_2$-coated ZnO slides was deduced from the TEM images which were taken using an FEI-Titan 300 electron microscope operating at 200 kV (HR-TEM, Hillsboro, OR, USA).

### *2.5. Energy-Dispersive X-ray Spectroscopy (EDX)*

The elemental analysis was conducted using EDX and HR-TEM.

### *2.6. Powder X-ray Diffraction Analysis (XRD)*

The powder X-ray diffraction analysis was performed using a Rigaku MiniFlex X-ray diffractometer (Japan, https://www.rigakuedxrf.com). The diffractogram recorded at 2θ, from 3° to 90°, and the instrument parameters were: target metal, Cu; filter, Kα; voltage, 45 kV; and current, 40 mA.

### *2.7. Size Distribution and Zeta Potential Analysis*

The particle size (z-average hydrodynamic diameter (nm)) and zeta potential (ζ) were measured by dynamic light scattering (DLS) and electrophoretic light scattering (ELS) performed on a Malvern zetasizer Nano ZS instrument (Malvern Instruments, UK). All measurements were performed at 25 °C after 120 s of temperature equilibration at a

backscattering angle of 173°. Using the Stokes–Einstein equation, the z-average hydrodynamic diameter (nm) was calculated from the diffusion coefficient. The zeta potential was calculated from the electrophoretic mobility using the Smoluchowski assumption. The z-average (nm) and ζ (mV) were reported as the mean of three replicates and standard deviation.

### *2.8. Diffuse Reflectance Spectroscopy (DRS)*

The absorption spectra of the $SiO_2$-coated ZnO slides were obtained by using the Kubelka–Munk conversion (K–M = $(1 - R)^2/2R$) of the recorded DRS spectra at room temperature for the solid samples on an FS5 spectrometer (Edinburgh, UK) equipped with a SC-30 (integrating sphere) as the sample holder. The specular reflection of the sample surface light was removed from the signal by directing the incident light at the sample at an angle of 0°; only the diffusive reflected light was measured. Polytetrafluoroethylene (PTFE) polymer was used as the reference. From the DRS spectra, the bandgap energy ($E_g$) values of the solid samples were calculated using $E_g = 1240$ eV nm $L^{-1}$, where l is the absorption edge (in nm).

### *2.9. Photoluminescence (PL) and Photoluminescence-Excitation (PLE) Measurements*

The PL spectra of the $SiO_2$-coated ZnO slides were recorded using an FS5 spectrometer (Edinburgh, UK) equipped with an SC-10 as the sample holder with a front-face geometry, which also utilized a Xenon lamp to excite the sample at 320 and 375 nm with long pass filters (LPFs) at 375 (or 395 nm) and 420 nm, respectively, which were placed between the sample holder and the emission monochromator. The excitation spectra were collected at 411 and 550 nm. All measurements were performed at two different temperatures, i.e., 263 and 298 K.

### *2.10. Variable-Temperature (VT) Measurements*

For the temperature variation experiments, a thermoelectrically cooled four-window cuvette holder was used together with an instrument software-powered controller to enable stable control of sample temperatures, from 263 to 378 K.

### *2.11. Excited-State PL Lifetime Measurements and Time-Resolved Photoluminescence (TRPL) Measurements*

The emission decays were measured by using a time-correlated single-photon counting (TCSPC)-based Edinburgh instrument (LifeSpec II spectrometer, Edinburgh, UK). The source used was either a picosecond diode laser with an $\lambda_{ex}$ of 375 nm with an instrument function of ~30 ps or a laser diode at 320 nm with an instrument function of ~90 ps and a specific LPF as described in the text; both sources were set at a repetition rate of 5 MHz. The PL decays were collected with a total count rate of 10,000 counts/s by using a red-sensitive high-speed PMT detector (H5773-04, Hamamatsu, Japan). The data were globally fitted to a tri-exponential model function convoluted with the appropriate instrument response function (IRF), utilizing a least squares statistical analysis (chi-square and residual plot were used to assess the goodness of fit). The average PL lifetime ($\overline{\tau}$) was calculated using $\overline{\tau} \sum_i f_i \tau_i$), where $f_i$ is the extracted fractional intensity contribution. The estimated experimental error was 2% for PL lifetime less than 1 ns and 20% for PL lifetime between 20 and 100 ns.

### *2.12. DAS Measurements*

For more adequate fitting, the emission decays collected every 10 nm over the entire emission spectra of $SiO_2$-coated ZnO slides with a dwell time of 10 s at each wavelength were globally fitted to a tri-exponential model function, and then convoluted with an instrument response function (IRF) of ~30 ps. The time-resolved data were specifically analyzed using the Edinburgh FAST software, in which decay-associated spectra (DAS)

were constructed from the extracted intensity-contribution fraction ($f_i$) calculated from the pre-exponential amplitudes ($B_i$), as follows:

$$I(t) = \sum_i B_i exp(-t/\tau_i) \quad (1)$$

$$f_i = \frac{B_i \tau_i}{\sum_j B_j \tau_j} \quad (2)$$

## 3. Results and Discussion

### *3.1. Material Characterizations of $SiO_2$-Coated ZnO Nanocrystals (Elements, Shape, Crystallography, Size Distribution, and Charges)*

Figure S1 in the Supporting Information shows the FTIR spectrum for the prepared $SiO_2$-coated ZnO slides as compared with those spectra for standard $SiO_2$ and ZnO powders as control samples. The characteristic bands at 3395 $cm^{-1}$ (ZnO), 3430 $cm^{-1}$ ($SiO_2$), and 3448 $cm^{-1}$ (sample) are attributed to the stretching vibration of intermolecular hydrogen bonds that exist between the adsorbed water molecules. The characteristic bands in ZnO at 1380 $cm^{-1}$ shifted in the $SiO_2$-coated ZnO nanocrystals to 1385 $cm^{-1}$, whereas the characteristic Si-O-Si asymmetry at 1097 $cm^{-1}$ observed in $SiO_2$ powder shifted to a new value at 1025 $cm^{-1}$. Additionally, the characteristic bands in $SiO_2$ at 1643 $cm^{-1}$ also shifted to 1596 $cm^{-1}$.

The surface morphologies of the $SiO_2$-coated ZnO nanocrystals were examined using transmission electron microscopy (TEM). Figure 1 shows a TEM image of the $SiO_2$-coated ZnO nanocrystals. The ZnO nanocrystals have a dense shell of $SiO_2$ coating their surface, with a thickness of about 75 nanometers, as measured by the TEM imaging. This size corresponds to that calculated from the XRD patterns and measured by DLS. To prove the presence of $SiO_2$, the elemental analysis of $SiO_2$-coated ZnO nanocrystals was carried out using energy dispersive spectroscopy (EDX). The EDX spectrum confirmed the presence of elements Zn, O, and Si in the prepared sample (Table 1). The carbon peak is due to the supporting substrate while collecting the TEM images or from the methanol solvent used in the preparation. Moreover, since the $SiO_2$-coated ZnO has 90 wt% silica, it is reflected in the higher atomic and weight percentages of Si as compared with Zn.

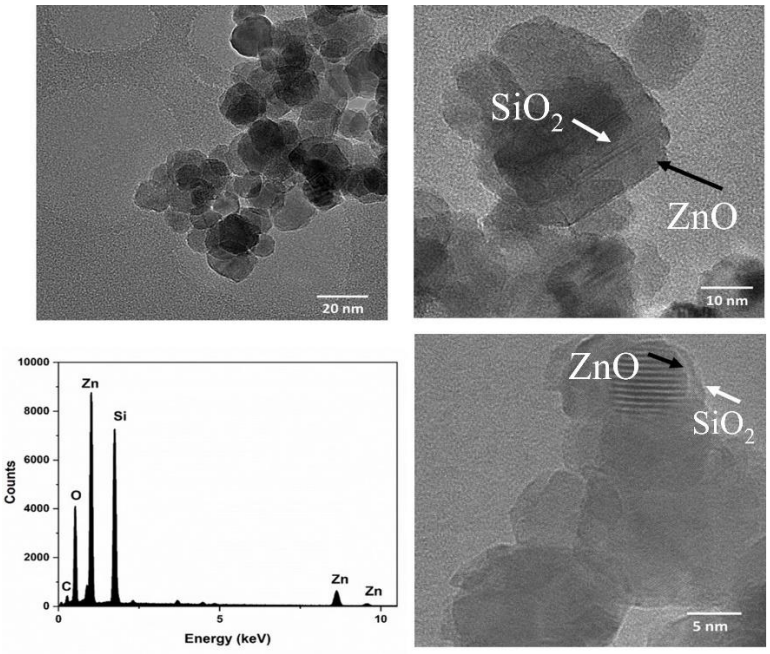



**Figure 1.** TEM images and the corresponding EDX spectrum of the $SiO_2$-coated ZnO nanocrystals.

**Table 1.** Weight and atomic percentages of the $SiO_2$-coated ZnO nanocrystals.

| Element | Weight % | Atomic % |
|---|---|---|
| Zn | 20.57 | 9.07 |
| Si | 61.17 | 62.73 |
| O | 15.42 | 27.77 |

The analyzed sample as a thin film on top of a glass plate under room temperature displays peaks less intense, but the diffraction patterns are specific and comparable (Figure S2 in the Supporting Information). The diffraction pattern of ZnO shows distinct and sharp peaks at 2θ values of 31.68°, 34.14°, 35.87°, 47.47°, 56.60°, 62.79°, and 67.92°. The broad peak at 2θ of around 20–30 corresponds to the amorphous silica. The diffraction pattern of the sample shows a unique pattern at 2θ values of 35.62°, 37.40°, 48.26°, 57.49°, 64.10°, and 68.95°.

The average size measured for the sample is 51.22 d. nm with a polydispersity index of 0.206. The zeta potential (ζ) value measured for the sample is −30.8 (Figure S3 in the Supporting Information).

### *3.2. Optical Properties of the $SiO_2$-Coated ZnO Nanocrystals*

By increasing the temperature of the $SiO_2$-coated ZnO slides from 263 K to 298 K, only the UV–visible absorption edge shifts from 335 to 355 nm, which corresponds to decreasing its optical bandgap from 3.7 to 3.5 eV (Figure 2), whereas the optical bandgap remains unchanged at 3.3 eV (375 nm).

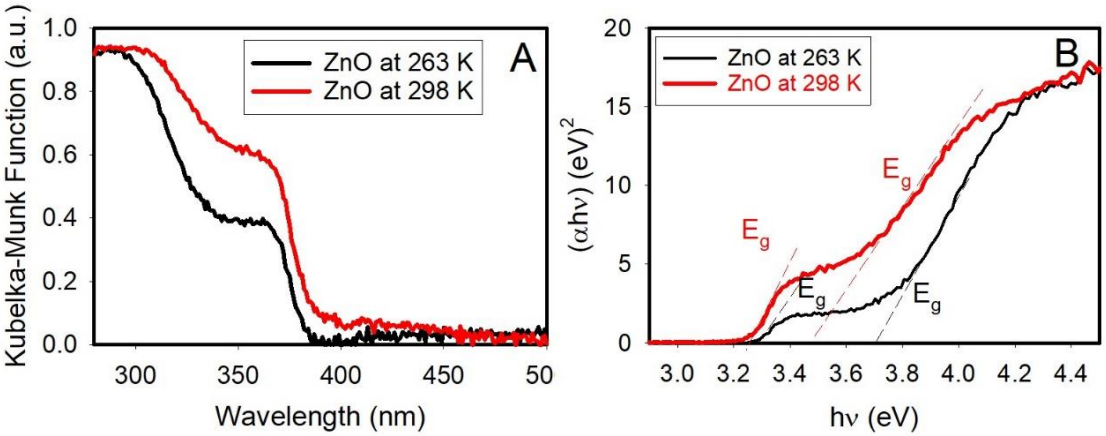



**Figure 2.** Diffusive reflectance spectra (DRS) (**A**); and the Tauc plots (**B**) of $SiO_2$-coated ZnO slides at 263 and 298 K (ambient temperatures) suggest direct optical bandgaps.

The measured photoluminescence (PL) and excitation spectra (PLE) of the $SiO_2$-coated ZnO samples (Figure S4 in the Supporting Information) confirm the presence of two electronic species [11–15], one emits at 385 nm (UV band), whose excitation spectrum has a maximum at 323 nm, and the other emits at 590 nm (yellow band) with an excitation peak position shifted from 323 to 348 nm as a shoulder. The results were confirmed by selective excitation of the yellow-emitted species at 375 nm instead of 320 nm, noting a higher intensity which was in agreement with the literature on similar nanocomposites [13]. Notably, the peak at 385 nm appeared at 400 nm because of the use of a long pass filter at 375 nm.

The measured PL spectra upon excitation at 320 nm of the $ZnO/SiO_2$ solid samples as a function of temperatures (Experimental Methods) reveal that, with an increase in the temperature from 263 to 378 K, the PL intensity decreases by one order of magnitude with a concomitant blue shift in the yellow emission peak position from about 590 to 575 nm (Figure 3A), while the UV peak at 385 nm (appeared at 411 nm when an LPF at 395 nm was used) remains unchanged. The results are confirmed by the selective excitation of the yellow

band at 375 nm (Figure 3B). The data, generated in multiple cycles, confirm nearly 100% restoration of the spectra with changes in temperature from 298 to 378 K (Figure 3C,D).

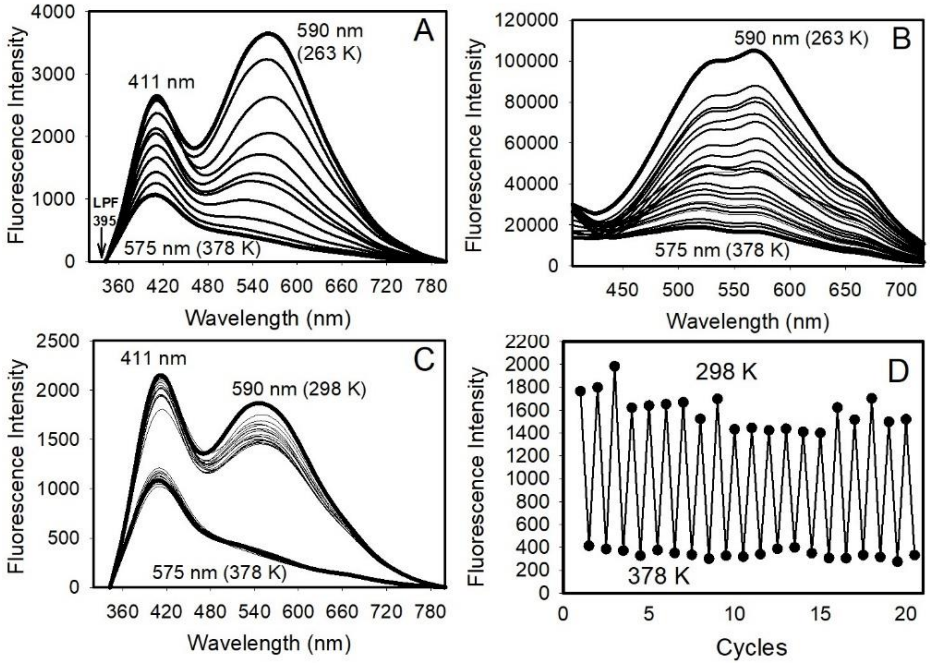



**Figure 3.** Photoluminescence (PL) spectra upon excitation at 320 nm (**A**) and 375 nm (**B**) at different temperatures from 263 to 378 K; (**C**) the data generated in several cycles from 298 to 378 K; (**D**) the corresponding plot monitored at 590 nm. Notably, the peak at 385 nm appeared at 411 nm because of the use of a long pass filter at 395 nm.

The emission decays were measured to better comprehend the nature of the fluorescent species in the solid state with decreasing temperature. The estimated excited-state PL lifetimes monitored at 411 and 541 nm when the samples were excited at 320 nm, respectively, at 298 K and 378 K, are listed in Table 2 and displayed in Figure 4. All emission traces were fitted to tri-exponential model functions after being convoluted with IRF (Experimental Methods).

**Table 2.** The observed excited-state PL lifetime for different ZnO–$SiO_2$ samples.

| Samples | $\lambda_{obs}$ (nm) | $\tau_1$ (ns) | $f_1$% | $\tau_2$ (ns) | $f_2$% | $\tau_3$ (ns) | $f_3$% | $\tau_{average}$ (ns) | Chi-Square |
|---|---|---|---|---|---|---|---|---|---|
| 298 K | 411 | 2.7 | 21 | 20 | 22 | 49.6 | 57 | 33 | 1.091 |
| 298 K | 541 | 1.4 | 28 | 12 | 15 | 111.5 | 57 | 66 | 1.041 |
| 378 K | 411 | 2.5 | 9 | 16.4 | 27 | 46.8 | 64 | 35 | 1.002 |
| 378 K | 541 | 0.81 | 52 | 7.03 | 14 | 67.55 | 34 | 24 | 1.061 |

The time resolution was ~90 ps and the excitation wavelength was 320 nm.

For comparison purposes, the estimated excited-state PL lifetimes from the decays monitored at 541 nm alone (Figure S5 in the Supporting Information) when the yellow-emitted species were selectively excited at 375 are compiled in Table S1 in the Supporting Information.

An analysis of the emission decays in Table 2 reveals no change in the average excited-state PL lifetime value (~33 ns) at 411 nm. In contrast, the average excited-state PL lifetime decreases at 541 nm (viz. from 66 to 24 ns, Table 2) with an increase in temperature from 298 to 378 K, indicating the generation of a new nonradiative channel, see below. Similar observations were confirmed upon the selective excitation of the 541 nm species (exciton) at 375 nm (viz. from 100 to 59 ns in Table S1, Supporting Information).

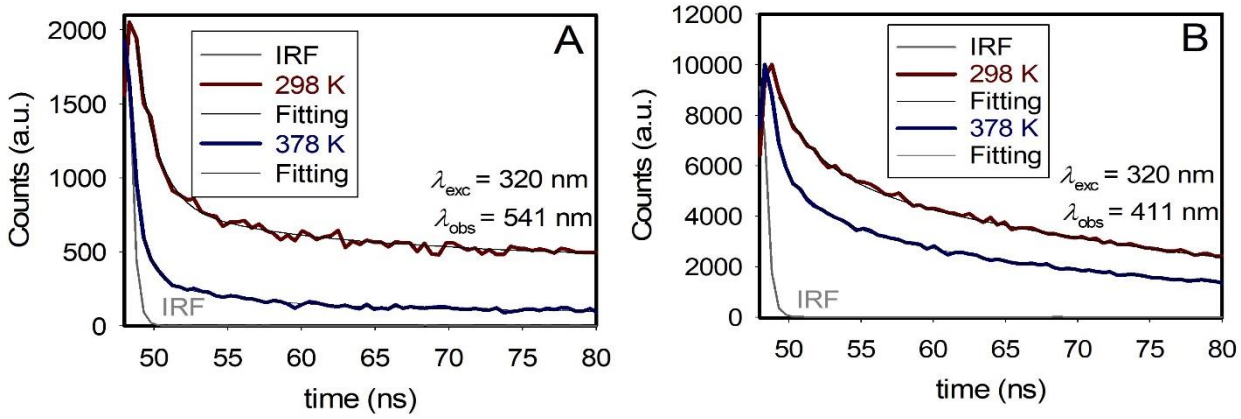



**Figure 4.** PL decays upon excitation at 320 nm monitored at the yellow band (**A**) and UV band (**B**) of ZnO–$SiO_2$ solids as a function of temperatures in kelvin (K). The exact monitoring wavelengths are indicated directly on the graph.

The DAS measurements more accurately indicate the effects of temperature on both the PL lifetime values and the contribution values of all components conducted globally at all wavelengths. It also helps us to assign each lifetime component to its DAS maximum (Table 3 and Figure S6 in the Supporting Information). It is observed that the PL lifetime values and amplitudes of the first two shorter Lifetimes **1** and **2** are not affected by temperature change (Table 3). However, the third component is solely affected by temperature. The decreased PL lifetime value (Table 3) and the decreased contribution of the third lifetime Component **3** (from 40 to 6%) confirm its population transfer through a nonradiative process, see below.

**Table 3.** Amplitudes and maxima of the decay-associated spectra (DAS) for the lifetime components of ZnO–$SiO_2$ solid films at different temperatures.

| Temperature | τ/ns Excited-State Lifetimes | | | DAS Maximum/nm | | | DAS Amplitudes | | | % of 3 |
|---|---|---|---|---|---|---|---|---|---|---|
| | 1 | 2 | 3 | 1 | 2 | 3 | 1 | 2 | 3 | |
| 263 K | 0.5 | 4 | 90 | <500 | <550 | 600 | 0.59 | 0.01 | 0.40 | 40 |
| 298 K | 0.8 | 6 | 92 | <500 | <550 | 600 | 0.50 | 0.20 | 0.30 | 30 |
| 378 K | 0.7 | 7 | 68 | <500 | <550 | 600 | 0.90 | 0.04 | 0.06 | 6 |

The origin of UV and visible emission of ZnO has been attributed to near band edge emission and intrinsic defects such as oxygen vacancies, respectively [11]. One report suggested that the decrease in the intensity of visible emission at 298 K has resulted when surface defects are effectively passivated by the $SiO_2$ [11]. Another research work reveals an increase in the exciton lifetime values in the presence of $SiO_2$ [20]. In the present work, we specifically observed temperature-dependent changes in the intensity of the visible emission for the first time in the presence of $SiO_2$.

The results also agree with DRS measurements at different temperatures in which the bandgap at 3.3 eV belongs to ZnO [1], while the bandgap at 3.7 eV, which is sensitive to temperature, is associated with the $SiO_2$-coated ZnO nanocrystals.

The % of Component **3** is calculated using the relation $\%3 = \frac{DAS\ amplitude for 3}{DAS\ amplitudes\ for 1+2+3}$. For the time-resolved fluorescence measurements, the time resolution was ~30 picoseconds and the excitation wavelength was 375 nm.

### *3.3. The Origin of Temperature-Dependent PL of ZnO/$SiO_2$ Nanomaterials*

PL temperature control of ZnO has already been reported by several researchers. Peng et al. studied the temperature-dependent photoluminescence properties of needle-like ZnO nanostructures and observed that the intensities of all transitions occurred in

near bandgap and visible regions and decreased with an increase in temperature along with the excitation power [23]. Moreover, Li et al. reported on exciton localization and stimulated emissions of ZnO nanocrystals and observed very weak visible emissions at low temperatures [24]. An inverse relation between PL with an increase in temperature was reported by Mhlongo et al. [25]. Bouzouraa et al. analyzed the surface property of ZnO and found that it was highly dependent on temperature [26]. It was later found that the morphological and optical properties of ZnO nanocrystals could further be tuned for optoelectronic device requirements by changing the processing temperature [27]. In another report on ZnO nanocrystals, it was observed that the temperature-dependent behavior of exciton transitions and oxygen vacancy recombinations [28] depended on temperature and decreased with an enhancement in the yellow band due to increasingly prominent localized bound exciton emissions.

Temperature control of PL from ZnO material upon coating by $SiO_2$ reveals, for the first time, the generation of thermally controlled nonradiative channel in ZnO-based nanocomposites. In general, nonradiative recombination processes that compete with radiative donor-acceptor recombination pair (DAP) emission from the emitting centers in solids can occur through either multiphoton emission (MPE) or energy transfer (Auger) processes [29]. In our ZnO-$SiO_2$ system, we confirm, for the first time, that the recombination of the free carriers via deep centers (DC) competes with the surface defect-assisted yellow emission. This is true because the capture process via DC is thermally activated as opposed to other nonradiative mechanisms [29].

## 4. Conclusions

In this study, we aimed at elucidating the effects of temperature on the photoluminescence from ZnO–$SiO_2$ nanocomposites. The formation of $SiO_2$-coated ZnO nanocrystals is confirmed by using several techniques such as FTIR, TEM, EDX, XRD, DLS, zeta potential, PL, PLE, TRPL, and the results elucidate the fundamental photophysical mechanism behind the efficient reversible switching of the yellow emission properties of $SiO_2$-coated ZnO nanocrystals by changing the ambient temperatures. Two emission bands at 385 and 590 nm are observed when the nanomaterials are excited at 325 nm. The UV and yellow bands are attributed to the radiative recombination (3.3 eV, ZnO) and surface defects (3.7 eV, ZnO–$SiO_2$). We confirm the contribution of the DC nonradiative recombination mechanism, for the first time, as an explanation for the decrease in yellow emission by increasing the temperature. The results pave the way for implementing these nanocomposites in the development of reversible optoelectronic devices with temperature control and for temperature-dependent photocatalytic applications.

**Supplementary Materials:** The following supporting information can be downloaded at: https://www.mdpi.com/article/10.3390/nano12193368/s1, Figure S1. FTIR spectra for (a) $SiO_2$-coated ZnO slides (b) $SiO_2$ powders (c) ZnO powders; Figure S2. The powder X-ray diffraction pattern of (A) Silica, (B) ZnO (C) our sample; Figure S3. Particle size distribution of the sample; Figure S4. Photoluminescence (PL) and excitation spectra at 298 K upon excitation at 375 nm and monitoring at 550 nm (dashed lines, a); and upon excitation at 320 nm and monitoring at 411 nm (solid lines, b); Figure S5. PL decays upon excitation at 375 nm monitored at the yellow band (590 nm) of ZnO–$SiO_2$ solids as a function of temperatures in kelvin (K); Table S1. The observed excited-state lifetime for different ZnO–$SiO_2$ samples; Figure S6. Decay-associated spectra (DAS) of a three-component mixture of exciton fluorophores for ZnO–$SiO_2$ solids at different temperatures upon excitation at 375 nm. The corresponding steady-state spectra of each solid are also shown for comparison (Section 2).

**Author Contributions:** Data curation and writing—original draft, N.K.; data curation and formal analysis, V.P.; data curation, Y.T.L.; formal analysis, F.C. and A.A.; data curation, S.A. and A.S.A.; conceptualization, data curation, formal analysis, funding acquisition; investigation, supervision, and writing—review and editing, N.S. All authors have read and agreed to the published version of the manuscript.

**Funding:** This research was supported by the UAE University/Zayed University Joint Research Program in the United Arab Emirates (grant number 12S106).

**Acknowledgments:** This research was supported by the UAE University/Zayed University Joint Research Program in the United Arab Emirates (grant number 12S106). A.A. acknowledges the National Water and Energy Center for its financial support (UAE University, grant no. 31R238).

**Conflicts of Interest:** The authors declare no conflict of interest.

## References

1. Ajmal, H.M.S.; Khan, F.; Nam, K.; Kim, H.Y.; Kim, S.D. Ultraviolet Photodetection Based on High-Performance Co-Plus-Ni Doped ZnO Nanorods Grown by Hydrothermal Method on Transparent Plastic Substrate. *Nanomaterials* **2020**, *10*, 1225. [CrossRef] [PubMed]
2. Pearton, S.J.; Norton, D.P.; Heo, Y.W.; Tien, L.C.; Ivill, M.P.; Li, Y.; Kang, B.S.; Ren, F.; Kelly, J.; Hebard, A.F. ZnO Spintronics and Nanowire Devices. *J. Electron. Mater.* **2006**, *35*, 862–868. [CrossRef]
3. Rahman, F. Zinc oxide light-emitting diodes: A review. *Opt. Eng.* **2019**, *58*, 010901. [CrossRef]
4. Shih, C.C.; Lee, W.Y.; Chiu, Y.C.; Hsu, H.W.; Chang, H.C.; Liu, C.L.; Chen, W.C. High-Performance Transparent Transistor Memory Devices Using Nano-Floating Gate of Polymer/ZnO Nanocomposites. *Sci. Rep.* **2016**, *6*, 20129. [CrossRef] [PubMed]
5. Wibowo, A.; Marsudi, M.A.; Amal, M.I.; Ananda, M.B.; Stephanie, R.; Ardy, H.; Diguna, L.J. ZnO Nanostructured Materials for Emerging Solar Cell Applications. *RSC Adv.* **2020**, *10*, 42838–42859.
6. Miccoli, B.; Cauda, V.; Bonanno, A.; Sanginario, A.; Bejtka, K.; Bella, F.; Demarchi, D. One-Dimensional ZnO/Gold Junction for Simultaneous and Versatile Multisensing Measurements. *Sci. Rep.* **2016**, *6*, 29763. [CrossRef] [PubMed]
7. Siddiqi, K.S.; Rahman, A. Properties of Zinc Oxide Nanoparticles and Their Activity Against Microbes. *Nanoscale Res. Lett.* **2018**, *13*, 141. [CrossRef]
8. Faizan, M.; Faraz, A.; Mir, A.R.; Hayat, S. Role of Zinc Oxide Nanoparticles in Countering Negative Effects Generated by Cadmium in Lycopersicon esculentum. *J. Plant. Growth Regul.* **2021**, *40*, 101–115. [CrossRef]
9. Sulciute, A.; Nishimura, K.; Gilshtein, E.; Cesano, F.; Viscardi, G.; Albert, G.N.; Ohno, Y.; Rackauskas, S. ZnO Nanostructures Application in Electrochemistry: Influence of Morphology. *J. Phys. Chem. C* **2021**, *125*, 1932–7447. [CrossRef]
10. Zhang, X.; Qin, J.; Xue, Y.; Yu, P.; Zhang, B.; Wang, L.; Liu, R. Effect of aspect ratio and surface defects on the photocatalytic activity of ZnO nanorods. *Sci. Rep.* **2014**, *4*, 4596. [CrossRef]
11. Zhao, S.; Ji, Z.; Yang, Y.; Huo, D.; Lv, Y. Nano-ZnO Embedded $SiO_2$ Glass with Intense Ultraviolet Emission. *Mater. Lett.* **2007**, *61*, 2547–2550. [CrossRef]
12. Xia, H.L.; Tang, F.Q. Surface Synthesis of Zinc Oxide Nanoparticles on Silica Spheres: Preparation and Characterization. *J. Phys. Chem. B* **2003**, *107*, 9175–9178.
13. Abdullah, M.; Shibamoto, S.; Okuyama, K. Synthesis of ZnO/$SiO_2$ Nanocomposites Emitting Specific Luminescence Colors. *Opt. Mater.* **2004**, *26*, 95–100.
14. Xiao, F.; Chen, R.; Shen, Y.Q.; Liu, B.; Gurzadyan, G.G.; Dong, Z.L.; Zhang, Q.Y.; Sun, H.D. Infrared Emission Properties and Energy Transfer in ZnO–$SiO_2$:Yb3+ Composites. *J. Alloys Compd.* **2011**, *509*, 7794–7797.
15. Hong, J.H.; Wang, Y.F.; He, G.; Wang, J.X. The Effect of Calcination Temperature on the Photoluminescence from Sol–Gel Derived Amorphous ZnO/Silica Composites. *J. Non-Cryst. Solids.* **2010**, *356*, 2778–2780.
16. An, S.S.A.; Yi, D.K.; Ramasamy, M.; Das, M. Role of Surface Modification in Zinc Oxide Nanoparticles and Its Toxicity Assessment toward Human Dermal Fibroblast Cells. *Int. J. Nanomed.* **2014**, *9*, 3707. [CrossRef]
17. Shimada, T.; Yasui, T.; Yonese, A.; Yanagida, T.; Kaji, N.; Kanai, M.; Nagashima, K.; Kawai, T.; Baba, Y. Mechanical Rupture-Based Antibacterial and Cell-Compatible ZnO/$SiO_2$ Nanowire Structures Formed by Bottom-Up Approaches. *Micromachines* **2020**, *11*, 610.
18. Ali, A.M.; Ismail, A.A.; Najmy, R.; Al-Hajry, A. Preparation and Characterization of ZnO–$SiO_2$ Thin Films as Highly Efficient Photocatalyst. *J. Photochem. Photobiol. A* **2014**, *275*, 37–46.
19. Meng, F.; Liu, Y.; Wang, J.; Tan, X.; Sun, H.; Liu, S.; Wang, S. Temperature dependent photocatalysis of g-$C_3N_4$, $TiO_2$ and ZnO: Differences in photoactive mechanism. *J. Colloid Interface Sci.* **2018**, *532*, 321–330. [CrossRef]
20. Shi, J.; Chen, J.; Feng, Z.; Chen, T.; Wang, X.; Ying, A.P.; Li, C. Time-Resolved Photoluminescence Characteristics of Subnanometer ZnO Clusters Confined in the Micropores of Zeolites. *J. Phys. Chem. B* **2006**, *110*, 25612–25618. [CrossRef]
21. Spanhel, L.; Anderson, M.A. Semiconductor Clusters in the Sol-Gel Process: Quantized Aggregation, Gelation, and Crystal Growth in Concentrated Zinc Oxide Colloids. *J. Am. Chem. Soc.* **1991**, *113*, 2826–2833. [CrossRef]
22. Hoyer, P.; Eichberger, R.; Weller, H. Spectroelectrochemical Investigations of Nanocrystalline ZnO Films, Berichte Bunsenges. *Für. Phys. Chem.* **1993**, *97*, 630–635.
23. Peng, D.; Chen, X.; Wang, Y.; Hu, Z.; Yu, K.; Zhu, Z. Temperature-dependent photoluminescence properties of needle-like ZnO nanostructures deposited on carbon nanotubes. *Appl. Phys. A* **2011**, *105*, 463–468.
24. Li, C.P.; Zhang, L.; Liu, C.J.; Gao, G. Exciton Localization and Stimulated Emission of ZnO Nanorods. *Key Eng. Mater.* **2013**, *538*, 161–164.
25. Mhlongo, G.H.; Motaung, D.E.; Nkosi, S.S.; Swart, H.C.; Malgas, G.F.; Hillie, K.T.; Mwakikunga, B.W. Temperature-Dependence on the Structural, Optical, and Paramagnetic Properties of ZnO Nanostructures. *Appl. Surf. Sci.* **2014**, *293*, 62–70.

26. Bouzouraa, M.B.; Battie, Y.; Dalmasso, S.; Zaïbi, M.A.; Oueslati, M.; En Naciri, A. Temperature Dependent Optical Properties of ZnO Thin Film Using Ellipsometry and Photoluminescence. *Superlattices Microstruct.* **2018**, *117*, 457–468.
27. Shakti, N.; Prakash, A.T.; Katiyar, M. Processing Temperature Dependent Morphological and Optical Properties of ZnO Nanorods. *Mater. Sci. Semicond. Process.* **2014**, *20*, 55–60. [CrossRef]
28. Meng, X.; Zhou, Y.; Zeng, X.; Chen, X.; Chu, Y. Oxygen Vacancy Mediated Temperature Dependent Emission Behavior of Localized Bound Excitons in ZnO Nanorods. *J. Lumin.* **2018**, *195*, 201–208.
29. Godlewski, M.; Zakrzewski, A. *Nonradiative Recombination Processes in II-VI Luminophores*; Jain, M., Ed.; University of Western Australia: Crawley, Australia, 2015.